Review Article

Nano Research
2023, 16(7): 9954–9967

ISSN 1998-0124 CN 11-5974/O4
https://doi.org/10.1007/s12274-023-5630-1

Application of high energy X-ray diffraction and Rietveld refinement in layered lithium transition metal oxide cathode materials

Zhuo Yang, Yong Lu, Xiaomeng Liu, Fujun Li, and Jun Chen (✉)

Renewable Energy Conversion and Storage Center (*RECAST*), *Key Laboratory of Advanced Energy Materials Chemistry* (*Ministry of Education*), *College of Chemistry*, *Nankai University*, *Tianjin 300071*, *China*

Received: 6 January 2023 / **Revised:** 27 February 2023 / **Accepted:** 28 February 2023

ABSTRACT

Layered lithium transition metal oxide (LTMO) cathode materials have attracted much attention for lithium-ion batteries and are shining in the current market. Establishing a clear structure–performance relationship is necessary for the performance improvement of LTMO cathode materials. The combination of synchrotron X-ray diffraction (XRD) with high intensity and XRD Rietveld refinement is powerful for revealing the structural characteristics of LTMO cathode materials. This review summarizes the application of high energy XRD and Rietveld refinement in LTMO cathode materials, including the brief introduction of synchrotron XRD and Rietveld refinement and their applications in understanding the structural evolution related to the synthetic, thermal runaway, cycling, and high-rate charge/discharge process of LTMO cathode materials. Synchrotron XRD can provide insights into the intermediates and reaction paths in the synthesis process, the origin of thermal runaway, the mechanism of structural decay during cycles, and the structural evolution during high-rate charging/discharging. Future works should focus on the development of higher intensity X-rays to gain more in-depth insights into the intrinsic relationship between their structural characteristics and properties.

KEYWORDS

synchrotron X-ray diffraction, Rietveld refinement, layered cathode materials, transition metal oxide, lithium-ion batteries

1 Introduction

Lithium-ion batteries (LIBs) have been widely used in portable electronic devices and electric vehicles (EVs) since their commercialization in 1991 [1–3]. The increasing popularity of portable electronic products and the rise of EVs in today's market have raised higher requirements for the performance of LIBs, especially regarding battery life, energy density, and cost [4, 5], which are largely determined by cathode materials. This urgently calls for development of low-cost and high-performance cathode materials for LIBs [6]. Among the candidates for cathode materials that have been considered and studied, the layered lithium transition metal oxide (LTMO) cathode materials are the most widely studied owing to their high theoretical capacity and low cost [7–9]. In particular, the LTMO cathode material $LiCoO_2$ has a theoretical specific capacity of 274 $mA{\cdot}h{\cdot}g^{-1}$, higher than that of $LiFeO_4$ with olivine structure (170 $mA{\cdot}h{\cdot}g^{-1}$) and $LiMn_2O_4$ with spinel (148 $mA{\cdot}h{\cdot}g^{-1}$) [8]. It is necessary and essential for rational microstructural design at the material level to truly unlock the potential of these LTMO cathode materials. In addition, the charge–discharge process of LTMO cathode materials for LIBs is complicated, which involves several simultaneous chemical and physical processes, such as structural evolution [10] and reactions both in the bulk and electrode/electrolyte interfaces [11]. There exist changes in lattice parameters, phase transition, and volume contraction/expansion upon lithium intercalation and de-intercalation at the cathode material level [12]. In order to design cathode materials with better performance and new electrochemistry, it is necessary to gain comprehensive and deep understanding of the intrinsic structural characteristics of LTMO cathode materials and the evolution of crystal structures in service.

X-ray diffraction (XRD) is a powerful and indispensable tool to reveal the structural characteristics of LTMO cathode materials owing to their high crystallinity [13]. It is worth mentioning that XRD can monitor and track the crystal structure evolution of cathode materials. However, to achieve real-time tracking of the dynamic evolution of the crystal structure of cathode materials during charge–discharge, XRD should have timely and spatial resolutions as high as possible. Compared with traditional laboratory diffractometers, synchrotron sources with the same principle have advantages in time-resolved (TR) studies due to their brightness, photon flux, penetration depth, and high collimation [14, 15]. High-resolution diffraction, especially synchrotron XRD, can offer high-quality structure refinement to distinguish very close lattice parameters and avoid severe peak overlapping. Rietveld refinement is a full spectrum linear fitting method proposed by Hugo M. Rietveld in 1967 [16]. It can reveal the distribution rules of atoms in the crystal cell, including important information such as atomic composition, atomic proportion, and atomic coordinates, and becomes an important tool for analyzing material structure [17, 18]. With the

Address correspondence to chenabc@nankai.edu.cn

development of synchrotron X-ray technology, it has been popularized to study various properties of LTMO cathode materials for LIBs by combining synchrotron XRD with Rietveld refinement [19]. Thus, systematical summary on the application of high energy XRD and Rietveld refinement in LTMO cathode materials is necessary and useful for future studies. Although there are some reviews about LTMO cathode materials for LIBs, the summary on synchrotron XRD and Rietveld refinement for LTMO cathode materials is still lacking [20–23].

Herein, we focus on summarizing the application of synchrotron XRD and Rietveld refinement in LTMO cathode materials. Firstly, we introduce the structural characteristics and properties of LTMO cathode materials. Next, synchrotron XRD and Rietveld refinement are introduced, and then their applications in LTMO are discussed from the perspective of the structure changes associated with synthesis, thermal runaway, cycling failing, and high-rate charge/discharge process. Finally, the shortcomings and future development of XRD Rietveld refinements in the structural analysis of LTMO cathode materials are discussed. This urges the development of higher intensity X-rays to gain more insights into the intrinsic relationship between structural characteristics and properties in the future.

2 Overview of LTMO cathode materials

The lattice structure of the LTMO cathode materials is closely related to battery performance such as power and energy density, cycle performance, and safety [24]. Figure 1(a) shows real-life LTMO cathode materials from battery-level applications to structure design of multiscale forms with atomic complexity. The space group of LTMO cathode material is $R\bar{3}m$, belonging to hexagonal system, with lithium, transition metal (TM), and oxygen occupying positions of 3*b*, 3*a*, and 6*c*, respectively [25]. Along the *c*-axis, Li-O and M-O octahedra are arranged alternately, forming two-dimensional channels for lithium transport [26]. The crystal structure of LTMO cathode materials is shown in Fig. 1(b). The representatives of LTMO cathode materials are $LiCoO_2$, $LiNi_xCo_y(Mn/Al)_{1-x-y}O_2$ ($0 \le x \le 1$ and $0 \le y \le 1$, NCM/A), as well as Li-rich cathode material $xLi_2MnO_3{\cdot}(1-x)LiTMO_2$ (TM = Ni, Co, and Mn), the structural characteristics and properties of which are summarized in Table 1 [22, 23, 27]. Among the LTMO cathode materials, $LiCoO_2$ is the first to be commercialized [27]. In addition, Ni-based LTMO materials, $LiNi_xCo_y(Mn/Al)_{1-x-y}O_2$, are showing promise in EVs [22, 28].

According to the crystal structure of LTMO, the spacing between the (003) crystal planes represents the diffusion channel of lithium. In other words, the larger the spacing between (003) crystal planes, the easier the lithium diffusion. At the same time, the change of *c*-axis of cell parameters also represents the size of layer spacing.

The lattice structure of LTMO cathode materials will expand and contract repeatedly during the charge–discharge cycles. The structure collapse, induced by many factors, such as current density and lithium removal, is the main factor for the poor cycling stability. Because lithium is transported in two-dimensional channels, the layer spacing is directly related to the rate performance. It is essential to clarify the correlation of the cycle stability and rate performance with the variation law of lattice parameters in the charge–discharge process. These problems are quite common in all the LTMO cathode materials [8]. Therefore, it is crucial to accurately characterize the change law of layer spacing driven by external field and the relationship between the interlayer spacing of lithium and its electrochemical

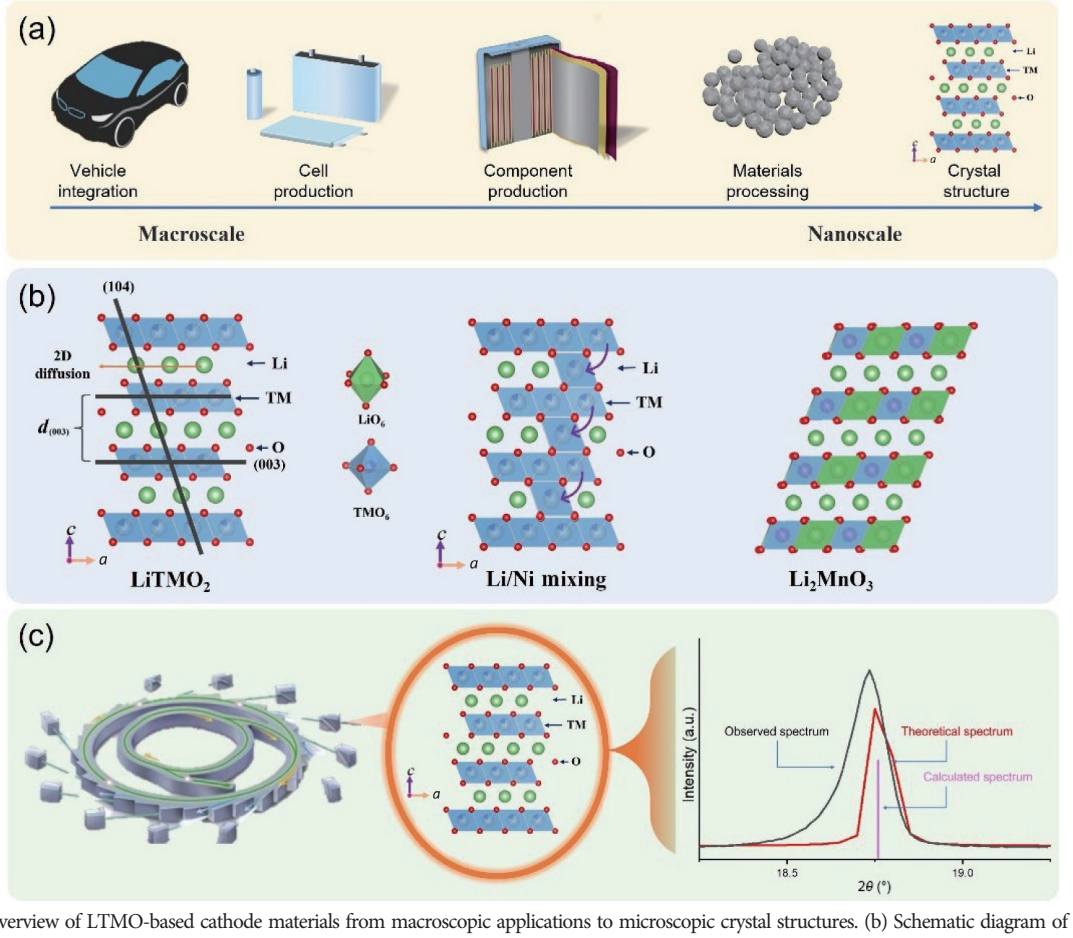

Figure 1 (a) Overview of LTMO-based cathode materials from macroscopic applications to microscopic crystal structures. (b) Schematic diagram of LTMO crystal structure. (c) Synchrotron XRD and Rietveld refinement used to study LTMOs.

Table 1 Structural characteristics and properties of layered cathode materials [22, 23, 27]

LTMO cathode materials	Space group	Atomic occupation			Theoretical specific capacity (mA·h·g^{-1})	Working voltage (V)
		Li	TM	O		
$LiCoO_2$	$R\bar{3}m$	3*b*	3*a*	6*c*	274	3.9
$LiNi_xCo_y(Mn/Al)_{1-x-y}O_2$	$R\bar{3}m$	3*b*	3*a*	6*c*	273–285	3.8
$xLi_2MnO_3{\cdot}(1-x)LiTMO_2$ $(0 < x < 1)$	$R\bar{3}m + C2/m$	2*b*/2*c*/4*h*	4*g*	4*i*/4*j*	273–350	3.8

properties. It is worth mentioning that compared with $LiCoO_2$, the Li/Ni mixing is an important factor affecting the cycling stability and rate performance of Ni-based LTMO cathode material.

In Ni-based LTMO materials, the similar radiuses of Ni^{2+} (0.69 Å) and Li^+ (0.76 Å) make it easy for Ni^{2+} to occupy position 3*b* and migrate into 3*a*, as shown in Fig. 1(b). It can be seen that TM ions are arranged in the (003) crystal plane. Compared with lithium, TM elements have stronger scattering ability for X-ray, so the diffraction of (003) crystal plane for X-ray is stronger and shows higher diffraction peak intensity. However, the diffraction of lithium for X-ray is very weak due to its small atomic number. When Li/Ni mixing occurs, a certain amount of lithium appears in the (003) crystal plane, which will weaken the diffraction peak of the (003) crystal plane and cause intensity decrease of the diffraction peak. For the (104) crystal plane, because of the appearance of TM in the lithium site, the increase of the total number of TM in the (104) crystal plane will enhance the diffraction intensity.

Li/Ni mixing will lead to a higher diffusion energy barrier for lithium ion in the LTMO cathode materials, because the Li/Ni mixing will reduce the Li-O layer spacing and increase the diffusion resistance [29]. At the same time, TM ions at the lithium site will also hinder the conduction of lithium ion. Hence, with the increase of Li/Ni mixing, the rate performance of the cathode material will be reduced. In addition, with the repeated charge–discharge cycles, the Li/Ni mixing becomes more severe and eventually results in capacity loss and cycling instability.

An in-depth and comprehensive understanding of the relationship between structure and performance in LTMO cathode materials is of great significance. XRD refinement is an important tool to study cell parameters. Their changes during cycles can be examined through XRD refinement, so as to provide insights into the lattice parameters and the degree of Li/Ni mixing in LTMO cathode materials in the charge and discharge process. The quality of refinement is strictly dependent on the time- and spatial-resolved X-ray.

3 Synchrotron XRD and Rietveld refinement

XRD originates from the discovery of M. Laue in 1912 that a crystalline material generates unique patterns of diffracted X-ray according to Bragg's law [30]. In short, diffraction occurs when Bragg's law is satisfied. Strong diffraction of X-rays through a crystal is detected at a certain X-ray wavelength and incident radiation angle. The Bragg's law can be described as Eq. (1)

$$n\lambda = 2d\sin\theta \quad (1)$$

where d is the inter-planar distance, θ is the scattering angle, n is an integer, and λ is the wavelength of the X-ray, respectively. In principle, the radiated X-rays are scattered by electrons around the atoms. The scattering coefficient of atoms is almost proportional to the number of electrons. Thus, light atoms are weak for X-ray scattering, while heavy atoms are strong.

XRD became an important means to study the structural characteristics of cathode materials for LIBs [31–33]. With the sustainable development of science and the progress of nuclear and high-energy physics, the neutron and synchrotron source and other large scientific facilities have been established. The brightness of the synchrotron X-ray spectrum is improved by 10 orders of magnitude compared with the approximately 10^9 photons·s^{-1}·mm^{-2}·mrad^{-2}·(0.1 BW)$^{-1}$ brightness of the Kα line of X-ray sources from the laboratory. The brightness of the third generation synchrotron radiation source can reach 10^{20} photons·s^{-1}·mm^{-2}·mrad^{-2}·(0.1 BW)$^{-1}$ [34]. In addition, synchrotron radiation X-ray has many advantages over traditional XRD, such as high signal-to-noise ratio and high intensity, which are listed in Table 2. The diffraction signals of high quality generated by the synchrotron X-ray in the crystal can be used to determine a variety of microstructure parameters with high precision, which greatly promotes the progress of LTMO cathode materials.

Any crystalline material has a specific phase composition and crystallographic parameters (such as space group, cell size, type of atoms in the cell, atomic arrangement, etc.). When X-ray enters a crystal and diffracts, a specific diffraction pattern is generated. The cell parameters determine the peak position and intensity of the XRD pattern. In other words, if the crystallographic parameters of materials are known, then the peak position and intensity can be calculated. However, if the sample displacement, background line shape, temperature factor, and preferred orientation are taken into account, the theoretical result of the materials is calculated with a certain peak shape function and a certain proportion. Note that the data obtained from XRD instrument are affected by multiple factors, such as instrument error and sample state, which will cause the error between the measured and calculated diffraction results. It is generally believed that the structure model obtained when the residual reaches the minimum is the real structure information of the sample.

Rietveld refinement is based on a specific crystal structure model and peak shape function to calculate the theoretical diffraction pattern within a certain angle range [16]. The calculated result is fitted to the measured diffraction data using the nonlinear least squares method. The residual difference (R) between the theoretical and the measured results is calculated. Usually, the smaller the R value, the better the fitting result and the more accurate the crystal structure analysis [35]. The commonly used R values are mainly the residual variance factor of the graph (R_p) and the residual variance factor of the weighted graph (R_{wp}), which are defined as follows

Table 2 Comparison of synchrotron radiation XRD with conventional XRD

XRD	Wavelength	Brightness (photons·s^{-1}·mm^{-2}·mrad^{-2}·(0.1 BW)$^{-1}$)	Intensity	Resolution	Signal-to-noise ratio
Synchrotron XRD	Tuneable	10^{17}–10^{20}	Strong	High	High
Conventional XRD	Specific	10^9	Weak	Low	Low

$$R_p = \sum |Y_{oi} - Y_{ci}| / \sum Y_{oi} \quad (2)$$

$$R_{wp} = \left[\sum W_i (Y_{oi} - Y_{ci})^2 / \sum W_i Y_{oi}^2\right]^{1/2} \quad (3)$$

where W_i is the statistical weight factor, Y_{oi} is the measured intensity value, and Y_{ci} is the calculated intensity value at point *i*.

In the refinement process, R_p and R_{wp} are often used to judge the reliability of Rietveld refinement results. The numerator in R_{wp} is a very small quantity calculated in the least squares fitting, which can accurately reflect the quality of the fitting. The change of R_{wp} in the refinement process indicates the refinement direction and is meaningful. The smaller the R_{wp}, the better the refinement results. In general, when the R_{wp} is less than 10%, the refinement result can be considered reliable.

However, it is not rigorous to judge the refinement results only based on the residual variance factor, because sometimes there will be a "pseudo-convergence" phenomenon. Therefore, while paying attention to R_{wp} in the refinement process, it is also necessary to focus on the chemical rationality of the refinement structure model, such as atomic proportions, atomic coordinates, etc. In the process of refining the LTMO cathode material of LIBs, the structure model can be established according to the results of inductively coupled plasma (ICP) test.

As shown in Fig. 1(c), synchrotron XRD and Rietveld refinement provide an opportunity to study the crystal structure of LTMO cathode materials. Detailed structure information of LTMO cathode materials can be obtained, such as layer spacing of lithium and degree of Li/Ni mixing. The relationship between structural characteristics and performance can be established. Therefore, combining synchrotron XRD with Rietveld refinement is effective to unlock the underlying structure information of LTMO cathode materials for LIBs.

4 Application of synchrotron XRD and Rietveld refinement in LTMO cathode materials

4.1 Structural evolution during the synthetic process

The performance of cathode materials for LIBs depends on their structural characteristics. The external driving force in the synthesis process is an important factor that directly affects structural characteristics [21, 36]. It is worth noting that the synthesis process of LTMO is a complicated chemical process, because it involves the reconstruction of atoms and the construction of new structures according to the precursors. For practical applications, synthetic control of stoichiometry and structure ordering is essential. But synthesis reactions often proceed via nonequilibrium pathways due to its inherent complexity [37]. It is important to understand the dynamic evolution behavior of structures, especially the capture of intermediates during synthesis. For Ni-based LTMO cathode materials, it is of great significance for the synthesis of perfectly ordered cathode materials to gain insights into the cation ordering in the synthesis process [38].

Synchrotron X-ray can take high-quality full-range XRD patterns in time scales of several seconds, thus fast and subtle changes in structure and composition can be tracked [39–41]. For example, the structural evolution in the process of synthesizing $LiCoO_2$, $LiNiO_2$, and $LiNi_{0.8}Co_{0.2}O_2$ with acetate as precursor was studied by combining *in-situ* synchrotron XRD with Rietveld refinement [42]. As shown in Fig. 2(a), the phase evolution in the Li-Co-O, Li-Ni-O, and Li-Ni-Co-O systems as a function of time and temperature was revealed via XRD Rietveld refinement. It can be seen intuitively that both Ni- and Co-based LTMOs ultimately crystallize into the same $R\bar{3}m$ layered structure with thermodynamic stability, which evolve with different metastable intermediates to the final equilibrium products. Specifically, the results show the existence of metastable spinel polymorphs of $Li_2Co_2O_4$ with a space group of $Fd\bar{3}m$, which was formed with an equilibrium reaction product Co_3O_4 at low temperature. When heated at high temperature, $Li_2Co_2O_4$ is smoothly transformed into the equilibrium layered $LiCoO_2$ phase. Li/Ni mixing is an inevitable challenge in Ni-based LTMO cathode materials. Figure 2(b) shows the proportion of TM in the lithium layer obtained in the three systems. As for the Li-Ni-Co-O system, the proportion of TM in the lithium layer is relatively high at low temperature, confirming that the disordered rock salt ($Li_x(Ni,Co)_{2-x}O_2$, $Fm\bar{3}m$) was formed as an intermediate. The rising temperature consequently leads to $Li_x(Ni,Co)O_2$ with high Li/Ni mixing. In addition, they confirmed that Co doped $LiNiO_2$ can reduce the temperature of its transition to hexagonal layered phase by means of *in-situ* synchrotron XRD and Rietveld refinement, because Co can nucleate at lower temperature [43].

Similarly, it has demonstrated the appearance of disordered rock salt phase $Li_m(Ni_{0.6}Co_{0.2}Mn_{0.2})_{1-m}O$ ($Fm\bar{3}m$) and layered non-stoichiometric intermediate $Li_{1-x}(Ni_{0.6}Co_{0.2}Mn_{0.2})_{1+x}O_2$ during the high-temperature synthesis of Ni-based LTMO materials $LiNi_{0.6}Co_{0.2}Mn_{0.2}O_2$ (NCM622) [44]. The phase transition process from the completely disordered rock salt phase $Li_m(Ni_{0.6}Co_{0.2}Mn_{0.2})_{1-m}O$ ($Fm\bar{3}m$) to the disordered layered phase $Li_{1-x}(Ni_{0.6}Co_{0.2}Mn_{0.2})_{1+x}O_2$ was thoroughly studied, and the results showed that the cell parameters *a* and *c* values of $Li_{1-x}(Ni_{0.6}Co_{0.2}Mn_{0.2})_{1+x}O_2$ decrease rapidly at the beginning of the transition from disorder to order (770–800 °C). This indicates that severe long-range cation disorder (Li/Ni) in the layered structure will lead to the increase of the average cell volume (*V*) and lattice parameters *a* and *c*. It is revealed that the reaction temperature is the key factor affecting the Li/Ni mixing in the Ni-based LTMO materials. Wang et al. systematically studied the influence of the temperature on the structure during the synthesis of $LiNi_{0.7}Co_{0.15}Mn_{0.15}O_2$ (NCM71515) with the help of *in-situ* synchrotron XRD [45]. As shown in Fig. 2(c), it can be seen that the influence of synthesis temperature on cation ordering and Li/Ni mixing is obvious. The quantitative structure analysis shows that complicated cation ordering and disordering processes occur simultaneously throughout the heat treatment process. Temperature is proved to be crucial for the kinetics of cation ordering. The highest ordering cathode material was obtained at 850 °C during the heat treatment of NCM71515 in air.

$LiCoO_2$ phases are primarily dominated by a metastable spinel structural motif with the same stoichiometry, whereas the Ni-based LTMO intermediates proceed through a disordered rock salt structure motif. In the synthesis of LTMO cathode materials, it is confirmed by synchrotron XRD and Rietveld refinement that the structure of intermediates plays a significant role in the structural characteristics of the final product. By elucidating the mechanisms driving the formation of nonequilibrium intermediates during solid-state synthesis, we can rationally control the processing at early stage or manipulation of precursors toward targeted structure motifs.

Compared with the solid-state synthesis for LTMO cathode materials [21, 46, 47], the microwave (MW) method has the advantages of short time and high efficiency [48–50]. This may provide an opportunity for rapid preparation of LTMO cathode materials. It is necessary to understand its structural evolution in the synthesis process, so as to accurately adjust the reaction conditions and synthesize cathode materials with perfectly layered structure. *In-situ* synchrotron XRD was employed to track the phase transition of $LiNi_{1/3}Mn_{1/3}Co_{1/3}O_2$ (NCM111) during microwave hydrothermal synthesis [51]. Figure 3(a) shows *in-situ*

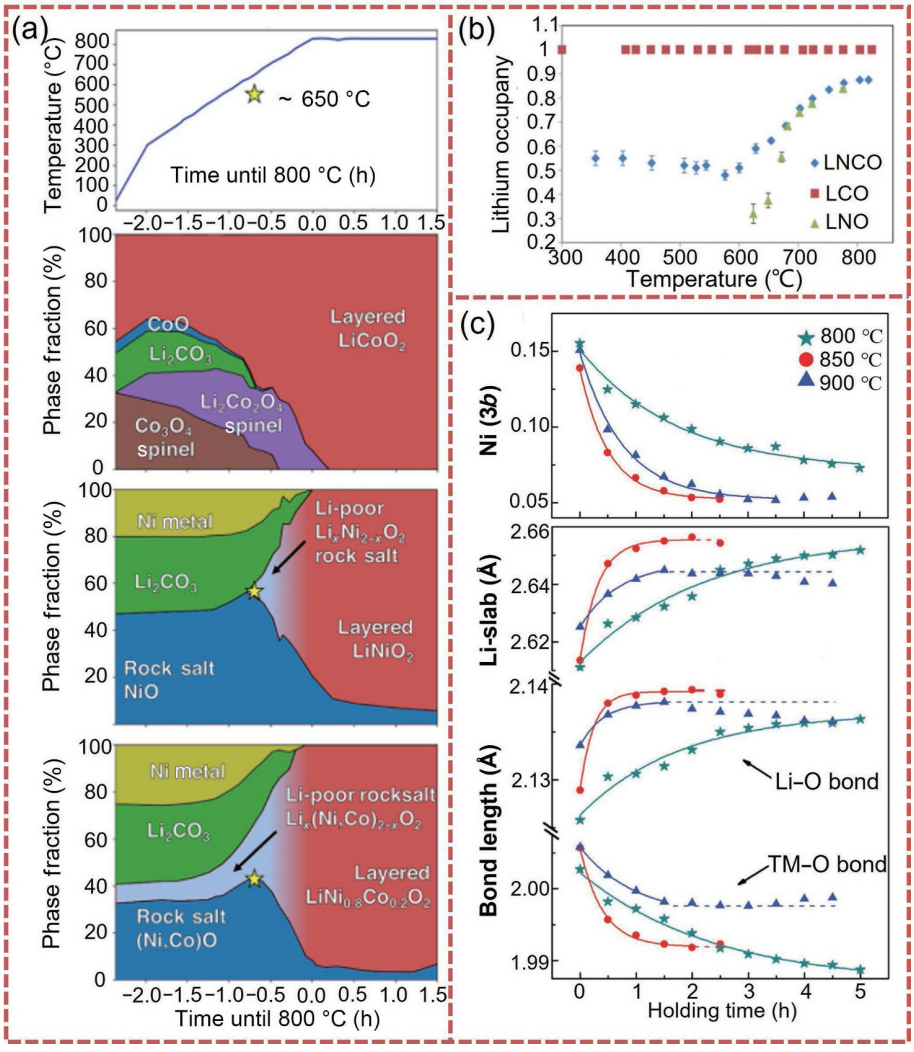

Figure 2 (a) Heating profile (top) and phase fractions (bottom) of crystalline phase in the Li-Co-O, Li-Ni-O, and Li-Ni-Co-O systems. (b) Lithium content at the Li site as a function of temperature during synthesis. Reproduced with permission from Ref. [42], © American Chemical Society 2020. (c) Evolution of lattice parameters of NCM71515 during heat treatment at 800, 850, and 900 °C: occupancy of Ni ions at position 3*b* (top), changes in the distance of the Li-slab (middle), and the lengths of Li–O and TM–O bonds (bottom). Reproduced with permission from Ref. [45], © WILEY-VCH Verlag GmbH & Co. KGaA, Weinheim 2017.

XRD for microwave hydrothermal synthesis. As shown in Fig. 3(b), it was found that the hydroxide precursor transformed into a layered oxide product at below 160 °C for less than 4 min. The reaction rates of solid-state synthesis, hydrothermal synthesis, and microwave hydrothermal synthesis of cathode materials were compared by temperature-resolved synchrotron XRD and Rietveld refinement, as shown in Fig. 3(c). It was found that the reaction rate of microwave hydrothermal synthesis was much higher than those of solid-state synthesis and hydrothermal synthesis. It reveals the targeted energy transmission mechanism of microwave ultrafine synthesis by synchrotron XRD and Rietveld refinement.

4.2 Structural evolution during thermal runaway process

In addition to the electrochemical performance of LIBs, the safety issues related to thermal abuse are also a major obstacle for practical applications [52]. The thermal stability of cathode materials plays a crucial role in the safety of LIBs [52–54]. Generally, high temperature will lead to structure changes of cathode materials, followed by thermal runaway of batteries [55]. Therefore, it is essential to understand the structural evolution of cathode materials in the process of thermal runaway, so as to fully understand its potential harm and mitigate the safety issue.

As the LTMO cathode material is charged, its lattice gradually expands. When the charged LTMO materials are heated, their structures evolve, leading to a series of safety-related side reactions with the electrolyte [56]. Especially for overcharged Ni-based LTMO, the reduction of Ni^{4+} to Ni^{2+} during the heating process will release oxygen, which will react with electrolytes and lead to severe thermal runaway [57, 58]. More importantly, inferior thermal stability of Ni-based LTMO materials leads to rapid chemical and structural degradation, which will not favor its application [59–61]. Accordingly, temperature-resolved synchrotron XRD and structure refinement are helpful to reveal the degradation and stability of Ni-based LTMO materials [62, 63]. Wu et al. used this technique to compare the phase transition behaviors of charged Ni-based LTMO cathodes $Li_xNi_{0.8}Co_{0.15}Al_{0.05}O_2$ ($x < 0.15$) and $Li_xNi_{1/3}Co_{1/3}Mn_{1/3}O_2$ ($x < 0.15$) at different temperatures to study their thermal stability. The results indicate that $Li_xNi_{1/3}Co_{1/3}Mn_{1/3}O_2$ and $Li_xNi_{0.8}Co_{0.15}Al_{0.05}O_2$ undergo structural transformation from layered phase to spinel phase, and then to rock salt phase. Specifically, the transition temperature of $Li_xNi_{1/3}Co_{1/3}Mn_{1/3}O_2$ to spinel phase is higher than that of the charged $Li_xNi_{0.8}Co_{0.15}Al_{0.05}O_2$, which confirms that the thermal stability of Ni-based LTMO decreases with the increase of Ni content [62]. Doping alien elements can significantly promote the thermal stability of Ni-based LTMO cathode materials, such as Mg and Zr [64].

As for Ni-based ternary solid solution LTMO cathode materials ($LiNi_xCo_yMn_{1-x-y}O_2$ (NCM)), elucidation of the role of each

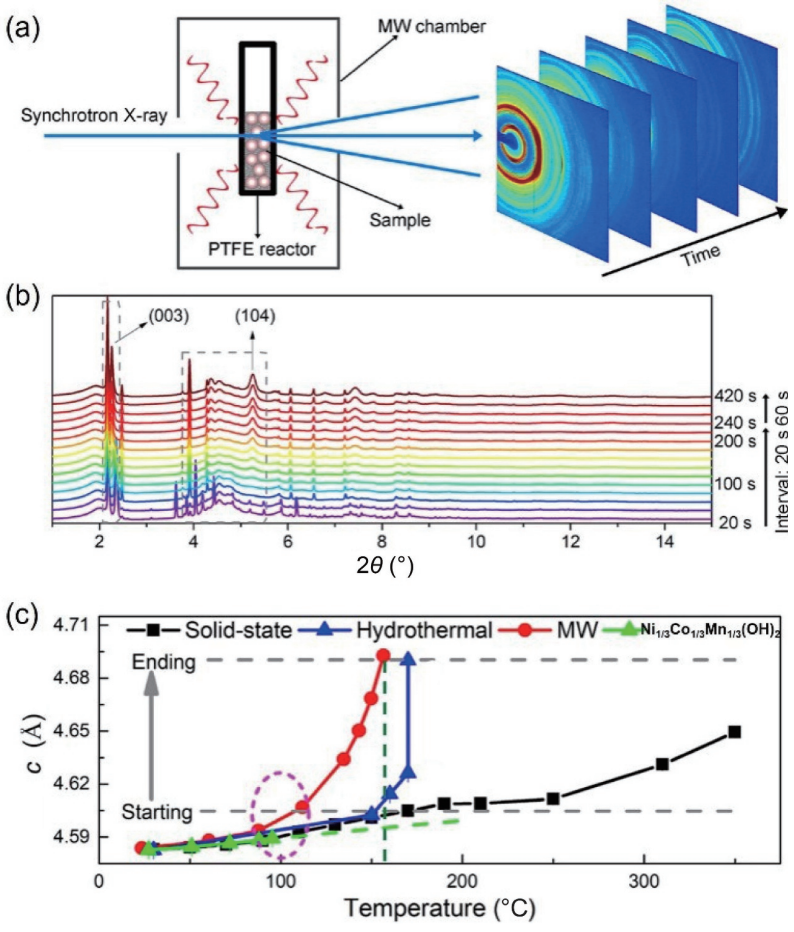

Figure 3 (a) Schematic illustration of fast synchrotron X-ray probing for the MW hydrothermal synthesis. (b) Time-resolved synchrotron XRD patterns during MW hydrothermal synthesis of NCM111. The temperature of the reaction vessel rose rapidly to 160 °C in the first 150 s, then dropped to ~ 125 °C and remained constant. (c) Lattice parameter *c* of the $Ni_{1/3}Co_{1/3}Mn_{1/3}(OH)_2$ precursor (green) as a function of temperature during solid-state synthesis (black), hydrothermal synthesis (blue), and MW hydrothermal synthesis (red). Reproduced with permission from Ref. [51], © Zhang, M. J. et al. 2020.

element in structure and performance is significant. It is generally believed that the existence and migration of Ni^{2+} in the lattice are the main reasons for the evolution from layer to rock salt phase during heating [52, 58]. It has been found that Mn maintains a constant +4 in the process of charge–discharge and occupies the octahedral sit in the TM layer to benefit the integrity of the layered structure and the thermal stability of Ni-based LTMO cathode materials [65, 66]. However, the role of Co element in the thermal stability of LTMO cathode materials is still unclear.

To investigate the roles of Co and Mn in terms of structure stability, synchrotron XRD was employed to study the structural characteristics of Co-rich and Mn-rich Ni-based LTMO materials [67]. After charged the battery to 4.4 V, as shown in Fig. 4(a), the charged cathode was disassembled in a glove box and loaded into a capillary with a heating device. Its structure changes were tracked by temperature-resolved synchrotron XRD. The heating rate was 10 °C·min^{-1}, and the resolution of the data material was 20 s·sheet^{-1}. Combined with Rietveld refinement, the function of crystalline phase content with temperature during heating was obtained. As shown in Figs. 4(b) and 4(c), the initial temperatures of layered (003) peak fading in both Co-rich and Mn-rich cathode materials are about 206 and 195 °C, respectively. However, it is worth noting that compared with Co-rich cathode, Ni^{2+} precipitates, the (003) peak declines, and the characteristic peaks of spinel phase appear at lower temperature. This confirmed that the TM migration in Mn-rich cathode materials can occur at lower temperatures, which means that the stability of the Mn-rich cathode materials is poorer than that of the Co-rich cathode materials.

4.3 Structural evolution during cycling process

The main reasons for the poor cycling stability of the LTMO cathode material are cracking and the loss of contact of active material due to large volume change during cycles [68]. The capacity attenuation of Ni-based LTMO cathode materials is also related to cation disorder in particle surface caused by Li/Ni mixing, resulting in structure transformation from the initial layered ($R\bar{3}m$) phase to cubic spinel ($Fd\bar{3}m$) phase, and then to rock salt ($Fm3m$) phase [69]. Impedance increases gradually with polarization, inducing reduced electrochemical reversibility.

Improving cycling stability of LTMO materials is related to the elucidation of their structure, morphology, composition, and local chemistry. For example, surface coating and lattice doping can stabilize the structure during charge–discharge [70–72]. Particle formation engineering, such as composition gradient [73], ordered primary particle filling [74], and single crystal [75], has also been shown to be effective to improve cycling stability. To truly promote the cycling stability of LTMO cathode materials, rational microstructure design at the electrode level is essential. Specifically, understanding of the lattice parameter variation of the electrode materials and the formation law of Li/Ni mixing in Ni-based material during the repeated charge–discharge process is of great importance. Real-time tracking of the changes of key lattice parameters in the charge–discharge process of LTMO is helpful to understand the degradation mechanism, and has important guiding significance for its structure stability and electrochemical performance [76]. *In-situ* XRD and Rietveld refinement are often applied to study the structural characteristics of cathode materials

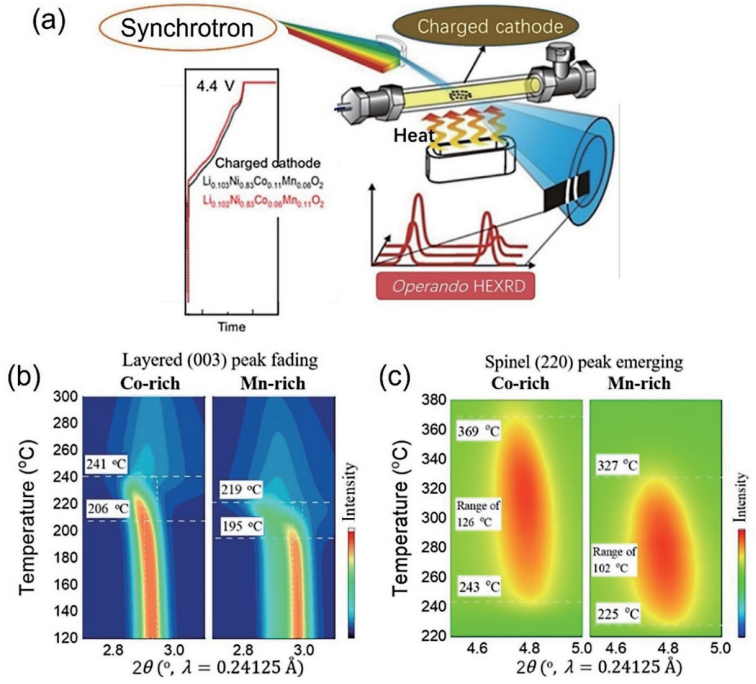

Figure 4 (a) Temperature-resolved synchrotron radiation XRD in combination with a mass spectrometer, on the left are the charge curves after 3 cycles of charge–discharge. (b) (003) diffraction peak fading and (c) (220) diffraction peak of spinel emerging during heating of Co-rich and Mn-rich cathodes. Reproduced with permission from Ref. [67], © American Chemical Society 2020.

during charge–discharge process, which can directly reveal the changes of lattice parameters and the degree of Li/Ni mixing [77–79].

There have been many reports on the variation trend of lattice parameters of LTMO cathode materials in the electrochemical process [80–83]. During the typical lithium extraction of LTMO, the unit parameter *c* increases first and then decreases, and the value of *a* decreases monotonically. The change of lattice parameters during discharge is reversible [73]. However, the crystal structure information obtained by laboratory XRD cannot fully explain the small changes in cell parameters. Therefore, synchrotron XRD with higher precision combined with Rietveld refinement is in need to track the changes of cell parameters of the LTMO during the electrochemical process [84–88]. Marker et al. obtained the cell parameters with higher precision of $LiNi_{0.8}Mn_{0.1}Co_{0.1}O_2$ (NCM811) cathode materials in the charge–discharge process by synchrotron XRD and Rietveld refinement [88]. Figure 5(a) shows the changes of lattice parameters *a* and *c* and unit cell volume of NCM811 during electrochemical lithium extraction. Throughout the charging process, the lattice parameter *a* decreases continuously from 2.87 to 2.81 Å. The lattice parameter *c* keeps rising before charging to 4.1 V, which proves that the O–O repulsive force increases the spacing between Li layers in the process of lithium removal. However, after charging to 4.1 V, the value of *c* decreases rapidly, indicating that the structure collapses. The change of cell volume is continuously decreasing, which is mild at the beginning stage. Combined with the change of *a*, it can be considered that the cell volume is initially controlled by *a* before ~ 4.1 V, and then shrinks faster, which further reflects the collapse of *c* lattice parameter. At the first discharge, all these lattice parameters are reversible. In addition, they defined the position of O in the direction of *c* as coordinate *Z*, and calculated the thickness changes of the Li and Ni layers through the coordinate *Z* value of O obtained by Rietveld refinement. As shown in Fig. 5(b), it can be seen that the O–O repulsion increases after lithium is removed, and the lithium layer expands. At the same time, the thickness of TM layer decreases, because the radius of Ni ion decreases and the covalence of Ni–O bond enhances with the charge increase of Ni ion. Therefore, the decline of *c* value at high voltage is caused by the further contraction of TM layer at the initial stage, followed by collapse of lithium layer at high voltage.

The mechanism of structure degradation of LTMO cathode materials was investigated by comparing the changes of lattice parameters during the first and following cycles. It was elucidated by *in-situ* synchrotron XRD combined with Rietveld refinement [89]. Figure 5(c) shows the *in-situ* XRD patterns of the 201st charge and discharge process. As shown in Fig. 5(d), the *c* value in the 201st cycle has little change, compared with the *c* value in the 1st charge process. In addition, the change of cell volume during the 201st charge and discharge process (2.0%) is nearly two times higher than that of the 1st charge and discharge process (1.1%). The large volume change may further aggravate the internal stress of the material and lead to deterioration of its cycle performance. The X-ray absorption near edge structure (XANES) spectroscopy results showed that the electrochemical attenuation of Li-rich LTMO was mainly caused by the asynchronous reaction between different transition metals and the chemo-mechanical instability.

Synchrotron XRD enables long-time *in-situ* experiments, that is, allows a cell to be studied without interruption over long cycles. The long duration of the experiment allows monitoring of changes over 1000 cycles. Chao et al. employed a modified cell for *in-situ* testing and analyzed the structure degradation mechanism of Ni-based LTMO materials NCM811 during charge and discharge with *in-situ* synchrotron XRD and Rietveld structure refinement [90]. The (003) peak splitting highlighted the presence of a fatigued phase at high charged state. Figure 5(e) shows the splitting of (003) diffraction peak, in which the two peaks represent the active and fatigued phases and the trough in the middle represents the intermediate phase of different charge states. It can be seen from Fig. 5(f) that the phase fraction of the fatigued phase increases substantially with the cycle number. The variation of cell parameter *c* during the cycle and the lattice mismatch rate were estimated to show that, when the charging exceeds a threshold of ~ 75%, there is a large lattice mismatch between the

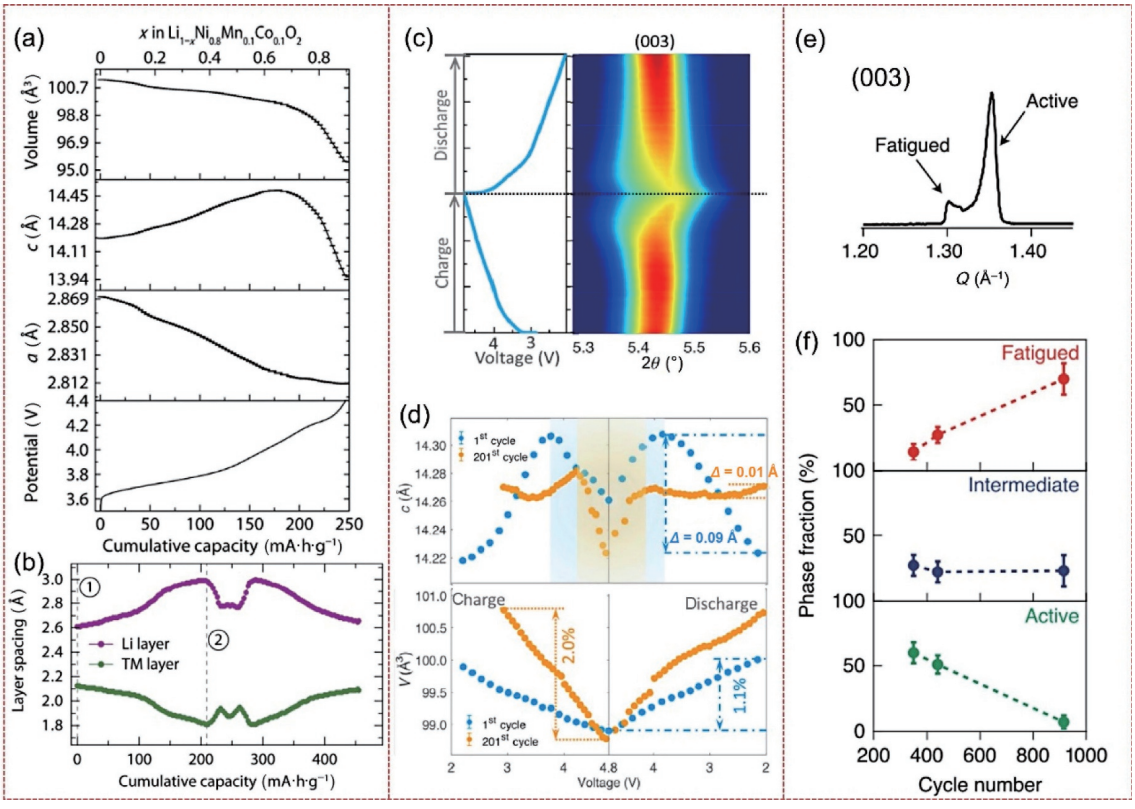

Figure 5 (a) Evolution of unit cell volume and lattice parameters *a* and *c* of NCM811 by Rietveld refinement during the first charge to 4.4 V. (b) Evolution of layer spacing during charge and discharge. Reproduced with permission from Ref. [88], © American Chemical Society 2019. (c) Charge–discharge curves and the corresponding contour plots of XRD patterns of Li-rich LTMO during the 201st cycle. Red to blue represents the decreasing peak intensity. (d) Lattice parameters (*c* and *V*) as a function of potential of Li-rich LTMO during the 201st cycle and the 1st cycle after electrode activation at 0.1 C. Reproduced with permission from Ref. [89], © Wang, L. G. et al. 2021. (e) Fatigued phase appears when (003) is split in NCM811 cathode after long cycles. (f) Fractions of crystalline phase (active, intermediate, and fatigued) obtained by refinement at different cycles. Reproduced with permission from Ref. [90], © Xu, C. et al. 2020.

layered structure and the surface reconstruction layer of rock salt phase. In addition, the unit cells of the layered structure contract significantly in both the *c* and *a*/*b* directions, resulting in a rapid and large increase in the lattice mismatch between the rock salt and the layered phases. This demonstrates that Ni-based LTMO cathode materials exhibit greater changes in lattice parameters (especially *c* parameter collapse) than the analogues with low Ni contents at the same upper limit voltage, making them more susceptible to fatigue degradation.

LTMO cathode materials are usually obtained as polycrystalline particles and composed of nanoscale primary particles. Anisotropic volume changes during lithium extraction/insertion make them inherently susceptible to grain boundary fracture, which leads to electrochemical performance degradation [8]. Compared with polycrystalline materials, single crystal cathode materials show advantages in the cycle stability by eliminating internal grain boundaries and crystalline fractures [75, 91–93]. It is meaningful to understand the lattice parameter changes of single crystal LTMO cathode materials during charge and discharge and then their cycling stability. Yang et al. compared the crystal structure evolutions of single crystal Li-rich LTMO cathode materials $Li(Li_{0.2}Ni_{0.2}Mn_{0.6})O_2$ (LLNMO-SC) and polycrystalline materials (LLNMO-PC) during extraction–insertion of lithium ion with *in-situ* time-resolved synchrotron XRD and Rietveld refinement [91]. Figures 6(a) and 6(b) are the refined patterns of LLNMO-PC and LLNMO-SC, where no impurity phases were found. The reasonably small residual variance factors *R*, R_p, and R_{wp} indicate that the fitting results are reliable. Rietveld refinements are shown in Figs. 6(c) and 6(d), indicating that during the first charge to 4.5 V, the cell parameters of LLNMO-PC and LLNMO-SC have the same change trend. However, from 4.5 to 4.8 V, the value of cell parameter *c* of LLNMO-PC changes significantly, while the *c* value of LLNMO-SC remains almost constant. Noteworthily, the changes of cell parameters *a*, *b*, *c*, and *V* of LLNMO-SC are much smaller than those of LLNMO-PC, which strongly confirms that single crystal materials have excellent structure reversibility and stability in the electrochemical cycles.

In addition to the evolution of structure parameters of LTMO cathode materials in the charge and discharge process explored by means of synchrotron XRD and Rietveld refinement for degradation, Li/Ni mixing is also an important factor affecting the cycling stability. It is necessary to understand its formation rule. The combination of synchrotron XRD with Rietveld refinement can accurately calculate the Li/Ni mixing proportion [69, 94–96]. Wang et al. proved that in NCM cathode materials, Co can significantly inhibit Li/Ni mixing, while Mn can aggravate Li/Ni mixing [95]. It is generally agreed that the Li/Ni mixing is usually attributed to the similar sizes of Ni^{2+} and Li^+, in other words, the higher the content of Ni^{2+}, the more the Li/Ni mixing. A linear relationship between the content of Ni^{2+} and Li/Ni mixing has been revealed.

Interestingly, Yin et al. employed synchrotron XRD to understand the Li/Ni mixing in NCM and were surprised to find that the concentration of Li/Ni mixing (labeled as $[Ni_{Li}]$) was not completely attributed to the ionic radius similarity between Ni^{2+} and Li^+ [96]. Figures 7(a)–7(c) show the dependence of $[Ni_{Li}]$ on (a) the average oxidation state of Ni, (b) the total content of Ni, and (c) the fractional concentration of Ni^{2+} on the total concentration of the transition metals (Ni, Mn, and Co). From the three graphs, it is clear that the graph with only Ni^{2+} fraction behaves monotonously. Figures 7(d)–7(f) show the percentage changes of Ni atoms located in the Li/Ni mixing (labeled as $\%Ni_{Li}$). The steady variation of $\%Ni_{Li}$ with composition indicates that the Li/Ni mixing concentration in these samples is mainly

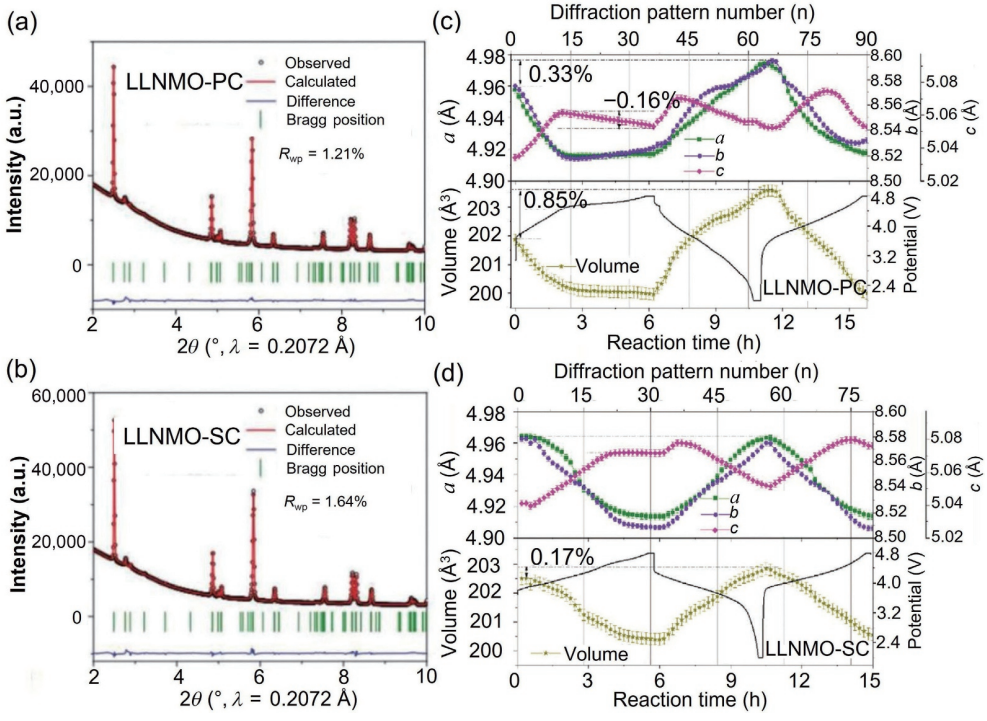

Figure 6 Synchrotron XRD Rietveld refinement patterns and changes of lattice parameters (*a*, *b*, *c*, and *V*) for (a) and (c) LLNMO-PC and (b) and (d) LLNMO-SC electrodes during charge and discharge. Reproduced with permission from Ref. [91], © Yang, X. X. et al. 2022.

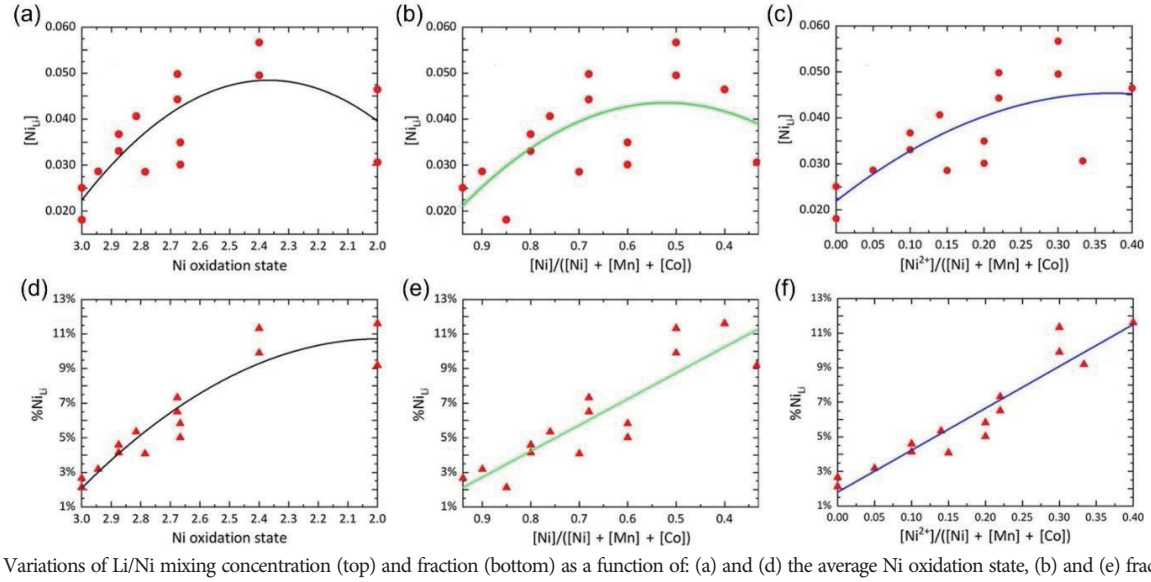

Figure 7 Variations of Li/Ni mixing concentration (top) and fraction (bottom) as a function of: (a) and (d) the average Ni oxidation state, (b) and (e) fraction of Ni (including both Ni^{2+} and Ni^{3+}) relative to all TMs, and (c) and (f) fraction of Ni^{2+} relative to all TMs for NCM samples, where solid line is the fitting result. Reproduced with permission from Ref. [96], © American Chemical Society 2019.

determined by thermodynamic rather than kinetic factors. The refinement results proved that the amount of Li/Ni mixing was related to the absolute number of Ni^{2+} (Fig. 7(f)) rather than the proportion of Ni^{2+} (Fig. 7(d)). It can be explained by the fact that Ni^{2+} ions, which are larger than the Ni^{3+} ions, push oxygen atoms out of the layer with transition metal ions in octahedral sites.

4.4 Structural evolution during high-rate charge/discharge process

In order to meet consumer demands, the batteries need to have high-rate capability, especially for charging. For the design of battery materials for high-rate applications, it is essential to clarify the structural evolution of electrode materials during fast charge–discharge [97, 98]. However, most of the researches are focused on the relatively slow processes near the thermodynamic equilibrium, not much are on the fast kinetics [10]. This is mainly due to the lack of fast data collection techniques with high signal-to-noise ratio. The synchrotron XRD with the characteristics of fast data acquisition and high brightness has become a powerful technique to study the structural dynamic behavior of electrode materials at high current densities [99, 100].

Zhou et al. employed TR-XRD to study the phase transition behavior of LTMO cathode materials $LiNi_{1/3}Mn_{1/3}Co_{1/3}O_2$ cycled at various charging rates (0.1, 1, 10, 30, and 60 C) [99]. It is shown that a different phase transition path is experienced in the high current charging process, in comparison with that in the low current charging process, that is, the intermediate phase appears at 10 C and becomes increasingly apparent at 30 and 60 C. The intermediate phase formed during high-rate charging is likely to act as buffer to reduce local stresses and strains caused by inhomogeneity during charging.

The structure degradation mechanism of NCM811 cathode at

different rates was studied by TR-XRD and Rietveld refinement [100]. The structure changes of the initial electrode and the electrode after 150 cycles at charging rates of 1 and 4 C were collected. As shown in Fig. 8, there is no obvious difference in the changing trends of cell parameters *a* and *c*. However, it is noticeable that whether it is the initial electrode or the electrode after 150 cycles, the cell volume change at 1 C charge is larger than that at 4 C. The larger volume change during the cycle may lead to the breakage of cathode material particles, increase of impedance, and generation of new interface side reactions, consequently resulting in capacity attenuation. This implies that the structural evolution of LTMO cathode materials dictates their high-rate performance.

5 Summary and outlook

In summary, this review focuses on the structural characteristics of LTMO cathode materials and the important role of synchrotron XRD and Rietveld refinement in elucidation of the complexity and evolution of their structural and chemical/electrochemical properties. It also provides new insights into mechanistic understanding of battery degradation and cathode material improvement, which are of significance for establishing the relationship between structural characteristics and performance. The application of synchrotron XRD and Rietveld refinement is discussed from the synthesis to thermal stability, cycling stability, and rate performance of LTMO materials, as summarized in Fig. 9. Specifically, the synthesis of Ni-based LTMO material and $LiCoO_2$ experienced rock salt phase and spinel phase intermediates, respectively. Co element has beneficial effect on thermal stability of NCM. The amount of Li/Ni mixing was related to the absolute number of Ni^{2+} rather than the proportion of Ni^{2+}. The charging at high rates usually leads to small change of cell volume.

Although synchrotron characterization techniques can provide valuable insights into LTMO cathode materials, there are still

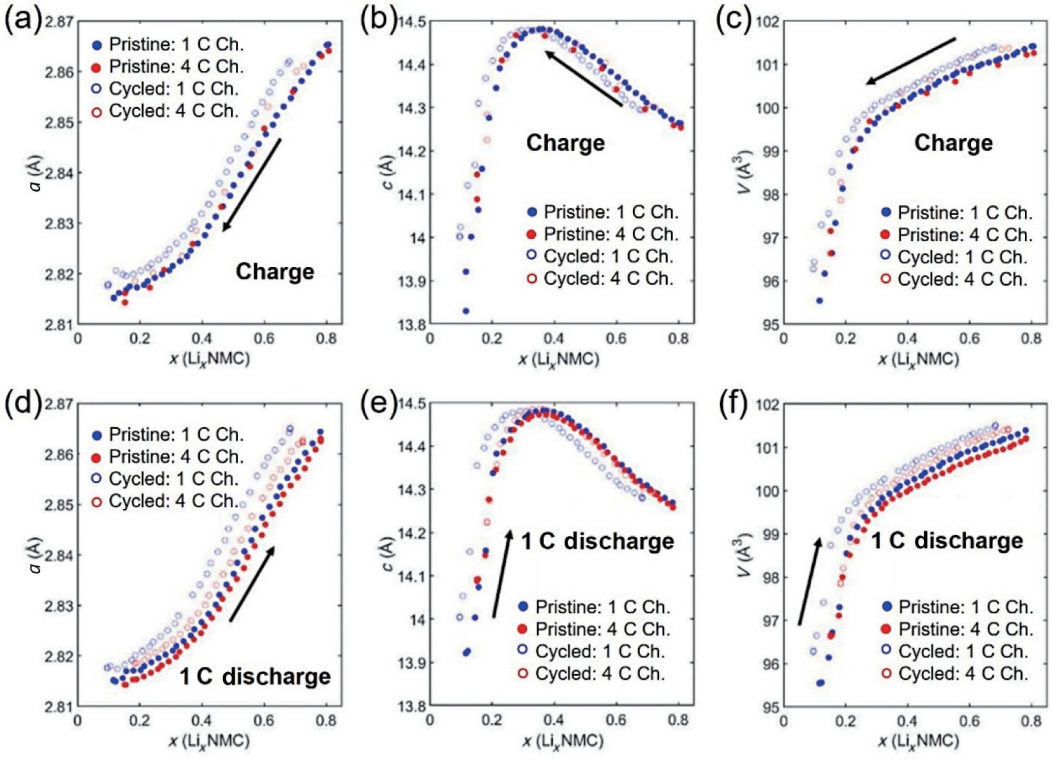

Figure 8 (a) and (d) Lattice parameter *a*, (b) and (e) lattice parameter *c*, and (c) and (f) unit cell volume of NCM811 cathode materials during charge and discharge at different currents by XRD Rietveld refinement. Reproduced with permission from Ref. [100], © The Electrochemical Society 2022.

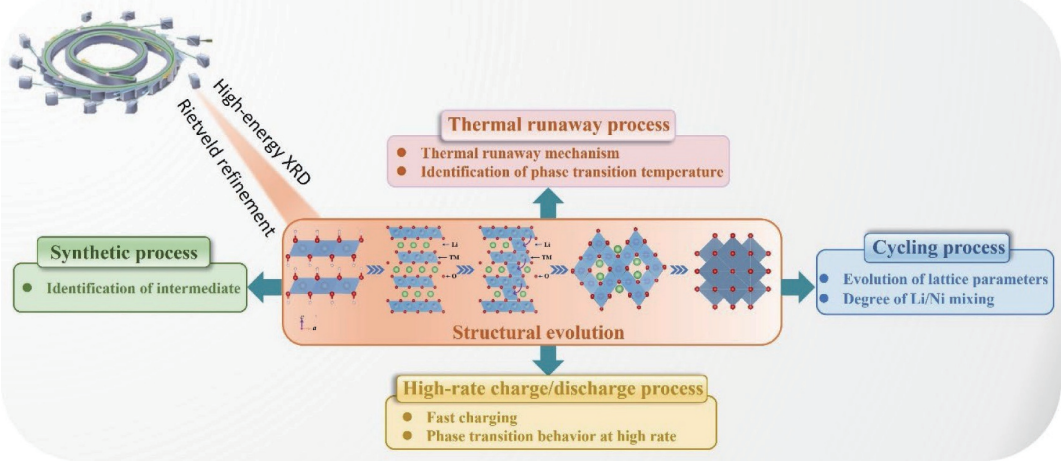

Figure 9 Summary on application of synchrotron XRD and Rietveld refinement in understanding structural evolution related to the synthesis, thermal stability, cycling stability, and rate performance of LTMO cathode materials.

some issues that need to be considered. For example, the spatial resolution of X-ray microscopy is usually limited to the level of a few to tens of nanometers. The synchrotron XRD Rietveld refinement usually reflects the average internal structure information of the materials and shows a little insufficient analysis of local fine structure information. It also provides limited ability to identify light elements (Li and O) and distinguish the elements with similar atomic numbers (such as Ni, Co, and Mn). These urge its combination with other techniques to better understand the structural characteristics of LTMO cathode materials.

For elucidation of the structural characteristics of LTMO cathode materials for LIBs, more investigations should focus on their dynamic behaviors. Firstly, high-performance area detectors with faster acquisition speeds (~ ms) can be employed for rapid time-resolved studies of the dynamic behavior of cathode materials, especially the evolution behavior of structures during synthesis and decay, such as the formation and evolution of metastable intermediates, which are neglected in conventional studies. This will provide key insights into the degradation and synthesis mechanisms of LTMO cathode materials. Secondly, enhanced X-ray brightness can promote X-ray experiments with unprecedented resolution and sensitivity, which is essential for the in-depth study of LTMO cathode materials. The development of high-energy X-ray technologies, such as the X-ray free electron laser (XFEL), will provide better spatial and temporal resolution [101]. New high-performance detectors can provide diffraction data with higher signal-to-noise ratio. Finally, the large amount of data obtained in *operando* cell experiments should be taken into account. With new collection techniques, it is possible to obtain large amounts of data in a very short period of time. Advanced refinement software based on the Rietveld method or the development of other new methods for refining large amounts of diffraction data should be required. In this regard, developing machine learning for data batch processing and analysis may be desirable in the future.

Acknowledgements

This work was supported by the National Natural Science Foundation of China (Nos. 22121005, 22020102002, and 21835004) and the Frontiers Science Center for New Organic Matter of Nankai University (No. 63181206).

References

[1] Armand, M.; Tarascon, J. M. Building better batteries. *Nature* **2008**, *451*, 652–657.

[2] Tarascon, J. M.; Armand, M. Issues and challenges facing rechargeable lithium batteries. *Nature* **2001**, *414*, 359–367.

[3] Reddy, M. V.; Mauger, A.; Julien, C. M.; Paolella, A.; Zaghib, K. Brief history of early lithium-battery development. *Materials* **2020**, *13*, 1884.

[4] Zeng, X. Q.; Li, M.; Abd El-Hady, D.; Alshitari, W.; Al-Bogami, A. S.; Lu, J.; Amine, K. Commercialization of lithium battery technologies for electric vehicles. *Adv. Energy Mater.* **2019**, *9*, 1900161.

[5] Guo, Y.; Wu, S. C.; He, Y. B.; Kang, F. Y.; Chen, L. Q.; Li, H.; Yang, Q. H. Solid-state lithium batteries: Safety and prospects. *eScience* **2022**, *2*, 138–163.

[6] Whittingham, M. S. Lithium batteries and cathode materials. *Chem. Rev.* **2004**, *104*, 4271–4302.

[7] Ye, Z. C.; Qiu, L.; Yang, W.; Wu, Z. G.; Liu, Y. X.; Wang, G. K.; Song, Y.; Zhong, B. H.; Guo, X. D. Nickel-rich layered cathode materials for lithium-ion batteries. *Chem.—Eur. J.* **2021**, *27*, 4249–4269.

[8] Huang, B.; Cheng, L.; Li, X. Z.; Zhao, Z. W.; Yang, J. W.; Li, Y. W.; Pang, Y. Y.; Cao, G. Z. Layered cathode materials: Precursors, synthesis, microstructure, electrochemical properties, and battery performance. *Small* **2022**, *18*, 2107697.

[9] Jamil, S.; Wang, G.; Fasehullah, M.; Xu, M. W. Challenges and prospects of nickel-rich layered oxide cathode material. *J. Alloys Compd.* **2022**, *909*, 164727.

[10] Pender, J. P.; Jha, G.; Youn, D. H.; Ziegler, J. M.; Andoni, I.; Choi, E. J.; Heller, A.; Dunn, B. S.; Weiss, P. S.; Penner, R. M. et al. Electrode degradation in lithium-ion batteries. *ACS Nano* **2020**, *14*, 1243–1295.

[11] Gauthier, M.; Carney, T. J.; Grimaud, A.; Giordano, L.; Pour, N.; Chang, H. H.; Fenning, D. P.; Lux, S. F.; Paschos, O.; Bauer, C. et al. Electrode–electrolyte interface in Li-ion batteries: Current understanding and new insights. *J. Phys. Chem. Lett.* **2015**, *6*, 4653–4672.

[12] Xu, C.; Reeves, P. J.; Jacquet, Q.; Grey, C. P. Phase behavior during electrochemical cycling of Ni-rich cathode materials for Li-ion batteries. *Adv. Energy Mater.* **2021**, *11*, 2003404.

[13] Zhu, W.; Liu, D. Q.; Paolella, A.; Gagnon, C.; Gariépy, V.; Vijh, A.; Zaghib, K. Application of *operando* X-ray diffraction and Raman spectroscopies in elucidating the behavior of cathode in lithium-ion batteries. *Front. Energy Res.* **2018**, *6*, 66.

[14] Lo, B. T. W.; Ye, L.; Tsang, S. C. E. The contribution of synchrotron X-ray powder diffraction to modern zeolite applications: A mini-review and prospects. *Chem* **2018**, *4*, 1778–1808.

[15] Lin, F.; Liu, Y. J.; Yu, X. Q.; Cheng, L.; Singer, A.; Shpyrko, O. G.; Xin, H. L.; Tamura, N.; Tian, C. X.; Weng, T. C. et al. Synchrotron X-ray analytical techniques for studying materials electrochemistry in rechargeable batteries. *Chem. Rev.* **2017**, *117*, 13123–13186.

[16] Rietveld, H. M. Line profiles of neutron powder-diffraction peaks for structure refinement. *Acta Cryst.* **1967**, *22*, 151–152.

[17] Malmros, G.; Thomas, J. O. Least-squares structure refinement based on profile analysis of powder film intensity data measured on an automatic microdensitometer. *J. Appl. Cryst.* **1977**, *10*, 7–11.

[18] Tlamsamania, D.; Ait-Mouha, M.; Slassi, S.; Khaddam, Y.; Zuluaga, D. L.; Yamni, K. Quantitative phase analysis of anhydrous clinker Portland using Rietveld method. *Rev. Inorg. Chem.* **2023**, *43*, 189–199.

[19] Bak, S. M.; Shadike, Z.; Lin, R. Q.; Yu, X. Q.; Yang, X. Q. *In-situ*/*operando* synchrotron-based X-ray techniques for lithium-ion battery research. *NPG Asia Mater* **2018**, *10*, 563–580.

[20] Qian, G. N.; Wang, J. Y.; Li, H.; Ma, Z. F.; Pianetta, P.; Li, L. S.; Yu, X. Q.; Liu, Y. J. Structural and chemical evolution in layered oxide cathodes of lithium-ion batteries revealed by synchrotron techniques. *Natl. Sci. Rev.* **2022**, *9*, nwab146.

[21] Malik, M.; Chan, K. H.; Azimi, G. Review on the synthesis of $LiNi_xMn_yCo_{1-x-y}O_2$ (NMC) cathodes for lithium-ion batteries. *Mater. Today Energy* **2022**, *28*, 101066.

[22] Xiang, J. W.; Wei, Y.; Zhong, Y.; Yang, Y.; Cheng, H.; Yuan, L. X.; Xu, H. H.; Huang, Y. H. Building practical high-voltage cathode materials for lithium-ion batteries. *Adv. Mater.* **2022**, *34*, 2200912.

[23] He, W.; Guo, W. B.; Wu, H. L.; Lin, L.; Liu, Q.; Han, X.; Xie, Q. S.; Liu, P. F.; Zheng, H. F.; Wang, L. S. et al. Challenges and recent advances in high capacity Li-rich cathode materials for high energy density lithium-ion batteries. *Adv. Mater.* **2021**, *33*, 2005937.

[24] Hu, E. Y.; Wang, X. L.; Yu, X. Q.; Yang, X. Q. Probing the complexities of structural changes in layered oxide cathode materials for Li-ion batteries during fast charge–discharge cycling and heating. *Acc. Chem. Res.* **2018**, *51*, 290–298.

[25] Xu, J.; Lin, F.; Doeff, M. M.; Tong, W. A review of Ni-based layered oxides for rechargeable Li-ion batteries. *J. Mater. Chem. A* **2017**, *5*, 874–901.

[26] Kang, K.; Ceder, G. Factors that affect Li mobility in layered lithium transition metal oxides. *Phys. Rev. B* **2006**, *74*, 094105.

[27] Ozawa, K. Lithium-ion rechargeable batteries with $LiCoO_2$ and carbon electrodes: The $LiCoO_2$/C system. *Solid State Ionics* **1994**, *69*, 212–221.

[28] You, B. Z.; Wang, Z. X.; Shen, F.; Chang, Y. J.; Peng, W. J.; Li, X. H.; Guo, H. J.; Hu, Q. Y.; Deng, C. W.; Yang, S. et al. Research progress of single-crystal nickel-rich cathode materials for lithium ion batteries. *Small Methods* **2021**, *5*, 2100234.

[29] Duan, Y. D.; Yang, L. Y.; Zhang, M. J.; Chen, Z. H.; Bai, J. M.; Amine, K.; Pan, F.; Wang, F. Insights into Li/Ni ordering and surface reconstruction during synthesis of Ni-rich layered oxides. *J. Mater. Chem. A* **2019**, *7*, 513–519.

[30] Bragg, W. L. The structure of some crystals as indicated by their diffraction of X-rays. *Proc. Roy. Soc. A: Math. Phys. Eng. Sci.* **191**, *89*, 248–277.

[31] Mai, Z. H. The discovery of X-ray diffraction by crystals and its great impact on science. *Physics* **2012**, *41*, 721–726.

[32] Xia, M. T.; Liu, T. T.; Peng, N.; Zheng, R. T.; Cheng, X.; Zhu, H. J.; Yu, H. X.; Shui, M.; Shu, J. Lab-scale *in-situ* X-ray diffraction technique for different battery systems: Designs, applications, and perspectives. *Small Methods* **2019**, *3*, 1900119.

[33] Reimers, J. N.; Dahn, J. R. Electrochemical and *in-situ* X-ray diffraction studies of lithium intercalation in Li_xCoO_2. *J. Electrochem. Soc.* **1992**, *139*, 2091–2097.

[34] Snigireva, I.; Snigirev, A. X-Ray microanalytical techniques based on synchrotron radiation. J. Environ. *Monit.* **2006**, *8*, 33–42.

[35] Thompson, P.; Cox, D. E.; Hastings, J. B. Rietveld refinement of Debye–Scherrer synchrotron X-ray data from Al_2O_3. *J. Appl. Cryst.* **1987**, *20*, 79–83.

[36] Zhu, L.; Fu, L.; Zhou, K. X.; Yang, L. X.; Tang, Z.; Sun, D.; Tang, Y. G.; Li, Y. X.; Wang, H. Y. Engineering crystal orientation of cathode for advanced lithium-ion batteries: A minireview. *Chem. Rec.* **2022**, *22*, e202200128.

[37] Martinolich, A. J.; Neilson, J. R. Toward reaction-by-design: Achieving kinetic control of solid state chemistry with metathesis. *Chem. Mater.* **2017**, *29*, 479–489.

[38] Weber, R.; Li, H. Y.; Chen, W. F.; Kim, C. Y.; Plucknett, K.; Dahn, J. R. *In-situ* XRD studies during synthesis of single-crystal $LiNiO_2$, $LiNi_{0.975}Mg_{0.025}O_2$, and $LiNi_{0.95}Al_{0.05}O_2$ cathode materials. *J. Electrochem. Soc.* **2020**, *167*, 100501.

[39] Wang, C. C.; Liu, L. J.; Zhao, S.; Liu, Y. C.; Yang, Y. B.; Yu, H. J.; Lee, S.; Lee, G. H.; Kang, Y. M.; Liu, R. et al. Tuning local chemistry of P2 layered-oxide cathode for high energy and long cycles of sodium-ion battery. *Nat. Commun.* **2021**, *12*, 2256.

[40] Hua, W. B.; Yang, X. X.; Casati, N. P. M.; Liu, L. J.; Wang, S. N.; Baran, V.; Knapp, M.; Ehrenberg, H.; Indris, S. Probing thermally-induced structural evolution during the synthesis of layered Li-, Na-, or K-containing 3d transition-metal oxides. *eScience* **2022**, *2*, 183–191.

[41] Qian, G. N.; Huang, H.; Hou, F. C.; Wang, W. N.; Wang, Y.; Lin, J. H.; Lee, S. J.; Yan, H. F.; Chu, Y. S.; Pianetta, P. et al. Selective dopant segregation modulates mesoscale reaction kinetics in layered transition metal oxide. *Nano Energy* **2021**, *84*, 105926.

[42] Bai, J. M.; Sun, W. H.; Zhao, J. Q.; Wang, D. W.; Xiao, P. H.; Ko, J. Y. P.; Huq, A.; Ceder, G.; Wang, F. Kinetic pathways templated by low-temperature intermediates during solid-state synthesis of layered oxides. *Chem. Mater.* **2020**, *32*, 9906–9913.

[43] Zhao, J. Q.; Zhang, W.; Huq, A.; Misture, S. T.; Zhang, B. L.; Guo, S. M.; Wu, L. J.; Zhu, Y. M.; Chen, Z. H.; Amine, K. et al. *In-situ* probing and synthetic control of cationic ordering in Ni-rich layered oxide cathodes. *Adv. Energy Mater.* **2017**, *7*, 1601266.

[44] Wang, S. N.; Hua, W. B.; Missyul, A.; Darma, M. S. D.; Tayal, A.; Indris, S.; Ehrenberg, H.; Liu, L. J.; Knapp, M. Kinetic control of long-range cationic ordering in the synthesis of layered Ni-rich oxides. *Adv. Funct. Mater.* **2021**, *31*, 2009949.

[45] Wang, D. W.; Kou, R. H.; Ren, Y.; Sun, C. J.; Zhao, H.; Zhang, M. J.; Li, Y.; Huq, A.; Ko, J. Y. P.; Pan, F. et al. Synthetic control of kinetic reaction pathway and cationic ordering in high-Ni layered oxide cathodes. *Adv. Mater.* **2017**, *29*, 1606715.

[46] Purwanto, A.; Yudha, C. S.; Ubaidillah, U.; Widiyandari, H.; Ogi, T.; Haerudin, H. NCA cathode material: Synthesis methods and performance enhancement efforts. *Mater. Res. Express* **2018**, *5*, 122001.

[47] Shi, Y.; Zhang, M. H.; Fang, C. C.; Meng, Y. S. Urea-based hydrothermal synthesis of $LiNi_{0.5}Co_{0.2}Mn_{0.3}O_2$ cathode material for Li-ion battery. *J. Power Sources* **2018**, *394*, 114–121.

[48] Tariq, H. A.; Abraham, J. J.; Shakoor, R. A.; Al-Qaradawi, S.; Abdul Karim, M. R.; Chaudhry, U. Synthesis of lithium manganese oxide nanocomposites using microwave-assisted chemical precipitation technique and their performance evaluation in lithium-ion batteries. *Energy Storage* **2020**, *2*, e202.

[49] Yang, G. J.; Park, S. J. Conventional and microwave hydrothermal synthesis and application of functional materials: A review. *Materials* **2019**, *12*, 1177.

[50] Kumar, R.; Sahoo, S.; Joanni, E.; Singh, R. K.; Kar, K. K. Microwave as a tool for synthesis of carbon-based electrodes for energy storage. *ACS Appl. Mater. Interfaces* **2022**, *14*, 20306–20325.

[51] Zhang, M. J.; Duan, Y. D.; Yin, C.; Li, M. F.; Zhong, H.; Dooryhee, E.; Xu, K.; Pan, F.; Wang, F.; Bai, J. M. Ultrafast solid–liquid intercalation enabled by targeted microwave energy delivery. *Sci. Adv.* **2020**, *6*, eabd9472.

[52] Liu, X.; Ren, D. S.; Hsu, H.; Feng, X. N.; Xu, G. L.; Zhuang, M. H.; Gao, H.; Lu, L. G.; Han, X. B.; Chu, Z. Y. et al. Thermal runaway of lithium-ion batteries without internal short circuit. *Joule* **2018**, *2*, 2047–2064.

[53] Zheng, J. X.; Liu, T. C.; Hu, Z. X.; Wei, Y.; Song, X. H.; Ren, Y.; Wang, W. D.; Rao, M. M.; Lin, Y.; Chen, Z. H. et al. Tuning of thermal stability in layered $Li(Ni_xMn_yCo_z)O_2$. *J. Am. Chem. Soc.* **2016**, *138*, 13326–13334.

[54] Shurtz, R. C.; Hewson, J. C. Review—Materials science predictions of thermal runaway in layered metal–oxide cathodes: A review of thermodynamics. *J. Electrochem. Soc.* **2020**, *167*, 090543.

[55] Feng, X. N.; Ren, D. S.; He, X. M.; Ouyang, M. G. Mitigating thermal runaway of lithium-ion batteries. *Joule* **2020**, *4*, 743–770.

[56] Nam, K. W.; Yoon, W. S.; Yang, X. Q. Structural changes and thermal stability of charged $LiNi_{1/3}Co_{1/3}Mn_{1/3}O_2$ cathode material for Li-ion batteries studied by time-resolved XRD. *J. Power Sources* **2009**, *189*, 515–518.

[57] Zhitao, E.; Guo, H. J.; Yan, G. C.; Wang, J. X.; Feng, R. K.; Wang, Z. X.; Li, X. H. Evolution of the morphology, structural, and thermal stability of $LiCoO_2$ during overcharge. *J. Energy Chem.* **2021**, *55*, 524–532.

[58] Bak, S. M.; Hu, E. Y.; Zhou, Y. N.; Yu, X. Q.; Senanayake, S. D.; Cho, S. J.; Kim, K. B.; Chung, K. Y.; Yang, X. Q.; Nam, K. W. Structural changes and thermal stability of charged $LiNi_xMn_yCo_zO_2$ cathode materials studied by combined *in-situ* time-resolved XRD and mass spectroscopy. *ACS Appl. Mater. Interfaces* **2014**, *6*, 22594–22601.

[59] Zhang, S. S. Problems and their origins of Ni-rich layered oxide cathode materials. *Energy Storage Mater.* **2020**, *24*, 247–254.

[60] Geldasa, F. T.; Kebede, M. A.; Shura, M. W.; Hone, F. G. Identifying surface degradation, mechanical failure, and thermal instability phenomena of high energy density Ni-rich NCM cathode materials for lithium-ion batteries: A review. *RSC Adv.* **2022**, *12*, 5891–5909.

[61] Jiang, M.; Danilov, D. L.; Eichel, R. A.; Notten, P. H. L. A review of degradation mechanisms and recent achievements for Ni-rich cathode-based Li-ion batteries. *Adv. Energy Mater.* **2021**, *11*, 2103005.

[62] Wu, L. J.; Nam, K. W.; Wang, X. J.; Zhou, Y. N.; Zheng, J. C.; Yang, X. Q.; Zhu, Y. M. Structural origin of overcharge-induced thermal instability of Ni-containing layered-cathodes for high-energy-density lithium batteries. *Chem. Mater.* **2011**, *23*, 3953–3960.

[63] Nam, K. W.; Bak, S. M.; Hu, E. Y.; Yu, X. Q.; Zhou, Y. N. N.; Wang, X. J.; Wu, L. J.; Zhu, Y. M.; Chung, K. Y.; Yang, X. Q. Combining *in-situ* synchrotron X-ray diffraction and absorption techniques with transmission electron microscopy to study the origin of thermal instability in overcharged cathode materials for lithium-ion batteries. *Adv. Funct. Mater.* **2013**, *23*, 1047–1063.

[64] Lipson, A. L.; Durham, J. L.; LeResche, M.; Abu-Baker, I.; Murphy, M. J.; Fister, T. T.; Wang, L. X.; Zhou, F.; Liu, L.; Kim, K. et al. Improving the thermal stability of NMC622 Li-ion battery

cathodes through doping during coprecipitation. *ACS Appl. Mater. Interfaces* **2020**, *12*, 18512–18518.

[65] Yabuuchi, N.; Kim, Y. T.; Li, H. H.; Shao-Horn, Y. Thermal instability of cycled $Li_xNi_{0.5}Mn_{0.5}O_2$ electrodes: An *in-situ* synchrotron X-ray powder diffraction Study. *Chem. Mater.* **2008**, *20*, 4936–4951.

[66] Noh, H. J.; Youn, S.; Yoon, C. S.; Sun, Y. K. Comparison of the structural and electrochemical properties of layered $Li[Ni_xCo_yMn_z]O_2$ (x = 1/3, 0.5, 0.6, 0.7, 0.8, and 0.85) cathode material for lithium-ion batteries. *J. Power Sources* **2013**, *233*, 121–130.

[67] Liu, X.; Xu, G. L.; Yin, L.; Hwang, I.; Li, Y.; Lu, L. G.; Xu, W. Q.; Zhang, X. Q.; Chen, Y. B.; Ren, Y. et al. Probing the thermal-driven structural and chemical degradation of Ni-rich layered cathodes by Co/Mn exchange. *J. Am. Chem. Soc.* **2020**, *142*, 19745–19753.

[68] Schweidler, S.; de Biasi, L.; Garcia, G.; Mazilkin, A.; Hartmann, P.; Brezesinski, T.; Janek, J. Investigation into mechanical degradation and fatigue of high-Ni NCM cathode material: A long-term cycling study of full cells. *ACS Appl. Energy Mater.* **2019**, *2*, 7375–7384.

[69] Zheng, J. X.; Ye, Y. K.; Liu, T. C.; Xiao, Y. G.; Wang, C. M.; Wang, F.; Pan, F. Ni/Li disordering in layered transition metal oxide: Electrochemical impact, origin, and control. *Acc. Chem. Res.* **2019**, *52*, 2201–2209.

[70] Cheng, Y.; Sun, Y.; Chu, C. T.; Chang, L. M.; Wang, Z. M.; Zhang, D. Y.; Liu, W. Q.; Zhuang, Z. C.; Wang, L. M. Stabilizing effects of atomic Ti doping on high-voltage high-nickel layered oxide cathode for lithium-ion rechargeable batteries. *Nano Res.* **2022**, *15*, 4091–4099.

[71] Qiu, Q. Q.; Yuan, S. S.; Bao, J.; Wang, Q. C.; Yue, X. Y.; Li, X. L.; Wu, X. J.; Zhou, Y. N. Suppressing irreversible phase transition and enhancing electrochemical performance of Ni-rich layered cathode $LiNi_{0.9}Co_{0.05}Mn_{0.05}O_2$ by fluorine substitution. *J. Energy Chem.* **2021**, *61*, 574–581.

[72] Zheng, J. C.; Yang, Z.; He, Z. J.; Tong, H.; Yu, W. J.; Zhang, J. F. *In-situ* formed $LiNi_{0.8}Co_{0.15}Al_{0.05}O_2$@$Li_4SiO_4$ composite cathode material with high rate capability and long cycling stability for lithium-ion batteries. *Nano Energy* **2018**, *53*, 613–621.

[73] Liu, T. C.; Yu, L.; Lu, J.; Zhou, T.; Huang, X. J.; Cai, Z. H.; Dai, A.; Gim, J.; Ren, Y.; Xiao, X. H. et al. Rational design of mechanically robust Ni-rich cathode materials via concentration gradient strategy. *Nat. Commun.* **2021**, *12*, 6024.

[74] Xu, Z. R.; Jiang, Z. S.; Kuai, C. G.; Xu, R.; Qin, C. D.; Zhang, Y.; Rahman, M. M.; Wei, C. X.; Nordlund, D.; Sun, C. J. et al. Charge distribution guided by grain crystallographic orientations in polycrystalline battery materials. *Nat. Commun.* **2020**, *11*, 83.

[75] Zhang, F.; Lou, S. F.; Li, S.; Yu, Z. J.; Liu, Q. S.; Dai, A.; Cao, C. T.; Toney, M. F.; Ge, M. Y.; Xiao, X. H. et al. Surface regulation enables high stability of single-crystal lithium-ion cathodes at high voltage. *Nat. Commun.* **2020**, *11*, 3050.

[76] Li, T. Y.; Yuan, X. Z.; Zhang, L.; Song, D. T.; Shi, K. Y.; Bock, C. Degradation mechanisms and mitigation strategies of nickel-rich NMC-based lithium-ion batteries. *Electrochem. Energy Rev.* **2020**, *3*, 43–80.

[77] Yu, H. X.; Qian, S. S.; Yan, L.; Li, P.; Lin, X. T.; Luo, M. H.; Long, N. B.; Shui, M.; Shu, J. Morphological, electrochemical, and *in-situ* XRD study of $LiNi_{0.6}Co_{0.2}Mn_{0.1}Al_{0.1}O_2$ as high potential cathode material for rechargeable lithium-ion batteries. *J. Alloys Compd.* **2016**, *667*, 58–64.

[78] Yang, X. Q.; McBreen, J.; Yoon, W. S.; Grey, C. P. Crystal structure changes of $LiMn_{0.5}Ni_{0.5}O_2$ cathode materials during charge and discharge studied by synchrotron based *in-situ* XRD. *Electrochem. Commun.* **2002**, *4*, 649–654.

[79] Wang, L.; Qiu, J. Y.; Wang, X. D.; Chen, L.; Cao, G. P.; Wang, J. L.; Zhang, H.; He, X. M. Insights for understanding multiscale degradation of $LiFePO_4$ cathodes. *eScience* **2022**, *2*, 125–137.

[80] Li, H.; Zhou, P. F.; Liu, F. M.; Li, H. X.; Cheng, F. Y.; Chen, J. Stabilizing nickel-rich layered oxide cathodes by magnesium doping for rechargeable lithium-ion batteries. *Chem. Sci.* **2019**, *10*, 1374–1379.

[81] Song, S. H.; Cho, M.; Park, I.; Yoo, J. G.; Ko, K. T.; Hong, J.; Kim, J.; Jung, S. K.; Avdeev, M.; Ji, S. et al. High-voltage-driven surface structuring and electrochemical stabilization of Ni-rich layered cathode materials for Li rechargeable batteries. *Adv. Energy Mater.* **2020**, *10*, 2000521.

[82] Chakraborty, A.; Kunnikuruvan, S.; Kumar, S.; Markovsky, B.; Aurbach, D.; Dixit, M.; Major, D. T. Layered cathode materials for lithium-ion batteries: Review of computational studies on $LiNi_{1-x-y}Co_xMn_yO_2$ and $LiNi_{1-x-y}Co_xAl_yO_2$. *Chem. Mater.* **2020**, *32*, 915–952.

[83] Lai, J.; Zhang, J.; Li, Z. W.; Xiao, Y.; Hua, W. B.; Wu, Z. G.; Chen, Y. X.; Zhong, Y. J.; Xiang, W.; Guo, X. D. Structural elucidation of the degradation mechanism of nickel-rich layered cathodes during high-voltage cycling. *Chem. Commun.* **2020**, *56*, 4886–4889.

[84] Liu, Y. C.; Zhu, H.; Zhu, H. K.; Ren, Y.; Zhu, Y. Z.; Huang, Y. L.; Dai, L.; Dou, S. M.; Xu, J.; Sun, C. J. et al. Modulating the surface ligand orientation for stabilized anionic redox in Li-rich oxide cathodes. *Adv. Energy Mater.* **2021**, *11*, 2003479.

[85] Matras, D.; Ashton, T. E.; Dong, H.; Mirolo, M.; Martens, I.; Drnec, J.; Darr, J. A.; Quinn, P. D.; Jacques, S. D. M.; Beale, A. M. et al. Emerging chemical heterogeneities in a commercial 18650 NCA Li-ion battery during early cycling revealed by synchrotron X-ray diffraction tomography. *J. Power Sources* **2022**, *539*, 231589.

[86] Sasaki, T.; Villevieille, C.; Takeuchi, Y.; Novák, P. Understanding inhomogeneous reactions in Li-ion batteries: *Operando* synchrotron X-ray diffraction on two-layer electrodes. *Adv. Sci.* **2015**, *2*, 1500083.

[87] Song, B. H.; Day, S. J.; Sui, T.; Lu, L.; Tang, C. C.; Korsunsky, A. M. Mitigated phase transition during first cycle of a Li-rich layered cathode studied by in *operando* synchrotron X-ray powder diffraction. *Phys. Chem. Chem. Phys.* **2016**, *18*, 4745–4752.

[88] Märker, K.; Reeves, P. J.; Xu, C.; Griffith, K. J.; Grey, C. P. Evolution of structure and lithium dynamics in $LiNi_{0.8}Mn_{0.1}Co_{0.1}O_2$ (NMC811) cathodes during electrochemical cycling. *Chem. Mater.* **2019**, *31*, 2545–2554.

[89] Wang, L. G.; Liu, T. C.; Dai, A.; De Andrade, V.; Ren, Y.; Xu, W. Q.; Lee, S.; Zhang, Q. H.; Gu, L.; Wang, S. et al. Reaction inhomogeneity coupling with metal rearrangement triggers electrochemical degradation in lithium-rich layered cathode. *Nat. Commun.* **2021**, *12*, 5370.

[90] Xu, C.; Märker, K.; Lee, J.; Mahadevegowda, A.; Reeves, P. J.; Day, S. J.; Groh, M. F.; Emge, S. P.; Ducati, C.; Layla Mehdi, B. et al. Bulk fatigue induced by surface reconstruction in layered Ni-rich cathodes for Li-ion batteries. *Nat. Mater.* **2021**, *20*, 84–92.

[91] Yang, X. X.; Wang, S. N.; Han, D. Z.; Wang, K.; Tayal, A.; Baran, V.; Missyul, A.; Fu, Q.; Song, J. X.; Ehrenberg, H. et al. Structural origin of suppressed voltage decay in single-crystalline Li-rich layered $Li[Li_{0.2}Ni_{0.2}Mn_{0.6}]O_2$ cathodes. *Small* **2022**, *18*, 2201522.

[92] Qian, G. N.; Zhang, Y. T.; Li, L. S.; Zhang, R. X.; Xu, J. M.; Cheng, Z. J.; Xie, S. J.; Wang, H.; Rao, Q. L.; He, Y. S. et al. Single-crystal nickel-rich layered-oxide battery cathode materials: Synthesis, electrochemistry, and intra-granular fracture. *Energy Storage Mater.* **2020**, *27*, 140–149.

[93] Langdon, J.; Manthiram, A. A perspective on single-crystal layered oxide cathodes for lithium-ion batteries. *Energy Storage Mater.* **2021**, *37*, 143–160.

[94] Wang, T.; Ren, K. L.; Xiao, W.; Dong, W. H.; Qiao, H. L.; Duan, A. R.; Pan, H. Y.; Yang, Y.; Wang, H. L. Tuning the Li/Ni disorder of the NMC811 cathode by thermally driven competition between lattice ordering and structure decomposition. *J. Phys. Chem. C* **2020**, *124*, 5600–5607.

[95] Wang, D. W.; Xin, C.; Zhang, M. J.; Bai, J. M.; Zheng, J. X.; Kou, R. H.; Peter Ko, J. Y.; Huq, A.; Zhong, G. M.; Sun, C. J. et al. Intrinsic role of cationic substitution in tuning Li/Ni mixing in high-Ni layered oxides. *Chem. Mater.* **2019**, *31*, 2731–2740.

[96] Yin, L.; Li, Z.; Mattei, G. S.; Zheng, J. M.; Zhao, W. G.; Omenya, F.; Fang, C. C.; Li, W. D.; Li, J. Y.; Xie, Q. et al. Thermodynamics of antisite defects in layered NMC cathodes: Systematic insights from high-precision powder diffraction analyses. *Chem. Mater.* **2020**, *32*, 1002–1010.

[97] Yang, Z. Z.; Charalambous, H.; Lin, Y. L.; Trask, S. E.; Yu, L.; Wen, J. G.; Jansen, A.; Tsai, Y.; Wiaderek, K. M.; Ren, Y. et al. Extreme fast charge aging: Correlation between electrode scale and heterogeneous degradation in Ni-rich layered cathodes. *J. Power Sources* **2022**, *521*, 230961.

[98] Wu, X. Y.; Song, B. H.; Chien, P. H.; Everett, S. M.; Zhao, K. J.; Liu, J.; Du, Z. J. Structural evolution and transition dynamics in lithium ion battery under fast charging: An *operando* neutron diffraction investigation. *Adv. Sci.* **2021**, *8*, 2102318.

[99] Zhou, Y. N.; Yue, J. L.; Hu, E. Y.; Li, H.; Gu, L.; Nam, K. W.; Bak, S. M.; Yu, X. Q.; Liu, J.; Bai, J. M. et al. High-rate charging induced intermediate phases and structural changes of layer-structured cathode for lithium-ion batteries. *Adv. Energy Mater.* **2016**, *6*, 1600597.

[100] Quilty, C. D.; West, P. J.; Wheeler, G. P.; Housel, L. M.; Kern, C. J.; Tallman, K. R.; Ma, L.; Ehrlich, S.; Jaye, C.; Fischer, D. A. et al. Elucidating cathode degradation mechanisms in $LiNi_{0.8}Mn_{0.1}Co_{0.1}O_2$ (NMC811)/graphite cells under fast charge rates using *operando* synchrotron characterization. *J. Electrochem. Soc.* **2022**, *169*, 020545.

[101] Ishikawa, T. Accelerator-based X-ray sources: Synchrotron radiation, X-ray free electron lasers, and beyond. *Philos. Trans. Roy. Soc. A:Math. Phys. Eng. Sci.* **2019**, *377*, 20180231.